Stochastic Dynamic Load Effect and Fatigue Damage Analysis of Drivetrains in Land-based and TLP, Spar and Semi-Submersible Floating Wind Turbines

Amir Rasekhi Nejad[a,b], Erin E. Bachynski[b,c,d], Marit I. Kvittem[a,b,e], Chenyu Luan[a,b], Zhen Gao[a,b,c], Torgeir Moan[a,b,c]

[a] *Norwegian Research Centre for Offshore Wind Technology (NOWITECH)*
[b] *Centre for Ships and Ocean Structures (CeSOS), Norwegian University of Science and Technology (NTNU)*
[c] *Centre for Autonomous Marine Operations and Systems (AMOS), NTNU*
[d] *MARINTEK, Trondheim, Norway*
[e] *DNV-GL, Oslo, Norway*

Abstract

This paper deals with the feasibility of using a 5 MW drivetrain which is designed for a land-based turbine, on floating wind turbines. Four types of floating support structures are investigated: spar, TLP and two semi-submersibles. The fatigue damage of mechanical components inside the gearbox and main bearings is compared for different environmental conditions, ranging from cut-in to cut-out wind speeds. For floating wind turbines, representative wave conditions are also considered. All wind turbines are ensured to follow similar power curves, but differences in the control system (integral to different concepts) are allowed. A de-coupled analysis approach is employed for the drivetrain response analysis. First, an aero-hydro-servo-elastic code is employed for the global analysis. Next, motions, moments and forces from the global analysis are applied on the gearbox multi body model and the loads on gears and bearings are obtained. The results suggest that the main bearings sustain more damage in floating wind turbines than on land-based. The highest main bearing damage is observed for the spar floating wind turbine. The large wave induced axial load on the main shaft is found to be the primary reason of this high damage in the spar wind turbine. Apart from the main bearings - which are located on the main shaft outside the gearbox - other bearings and gears inside the gearbox hold damages in floating wind turbines equal or even less than in the land-based turbine. It is emphasized that the results presented in this study are based on a drivetrain with two main bearings, which considerably reduces the non-torque loads on

E-mail address: Amir.Nejad@ntnu.no (Amir Rasekhi Nejad).

Prof. Jørgen Juncher Jensen serves as editor for this article.

the gearbox.

Keywords: Floating Wind Turbine, Drivetrain, Wind Turbine Gearbox, Wind Turbine Fatigue

1. Introduction

In recent years, there has been an increasing interest in extracting energy from offshore wind, primarily due to the high mean wind speed and steady wind conditions. The offshore wind energy research and development has shifted from the shallow water bottom-fixed wind turbines to deeper waters with floating turbines. The first major floating wind turbine prototype, Hywind, was installed in 2009 off the coast of Norway and the second one, WindFloat, in 2011 in Portugal. While there are many studies on the structural loads and their effects on floating wind turbines (e.g. [1, 2, 3, 4]), limited drivetrains' studies have been published. Among the few studies on this subject, Xing et al. [5] and Nejad et al. [6] found higher load effects in some of the mechanical components in spar type wind turbines compared to land-based turbines.

The gearbox is yet the dominant technology in wind turbine drivetrains with market share above 85% [7]. The current wind turbine gearbox design is based on the IEC 61400-4 [8] which does not address the floating wind turbines. On the gearbox component level, Dong et al. [9], Nejad et al. [10] and Jiang et al. [11] have investigated the gear contact fatigue, gear tooth root bending fatigue and bearing contact fatigue in wind turbine drivetrains respectively. However, all these studies were based on land-based or bottom-fixed wind turbines, and not floating turbines.

A main research question is then whether it is possible to use the drivetrains designed for land-based wind turbines on the floating ones. This paper addresses this question and aims to identify the most drivetrain-friendly floating wind turbine. To achieve this, a 5 MW three stage reference gearbox [12] is considered for a land-based, spar, TLP and two semi-submersibles wind turbines. Both global response analysis of these wind turbine concepts and local response analysis of the drivetrain are carried out. The fatigue damage of gears and bearings in floating wind turbines is then compared with the fatigue damage of the land-based turbines in different environmental conditions.

Post-Print Version. Original: https://doi.org/10.1016/j.marstruc.2015.03.006

2. Wind Turbines and Drivetrain Models

2.1. Wind Turbine Models

A land-based and four floating wind turbines (FWTs) are considered in the present study: a spar platform, a tension leg platform (TLP), and two semi-submersibles, as depicted in Figure 1. The FWTs are summarized in Table 1. The same platforms have been previously investigated with attention to the effects of fault in the blade pitch controller [13] and to the effects of misalignment between the wind and waves [14]. All of the models were assumed to support the NREL 5 MW wind turbine [15] with the OC3 Hywind tower [16]. Each of the platforms and their respective numerical models are described in greater detail in sections 2.1.1-2.1.5.

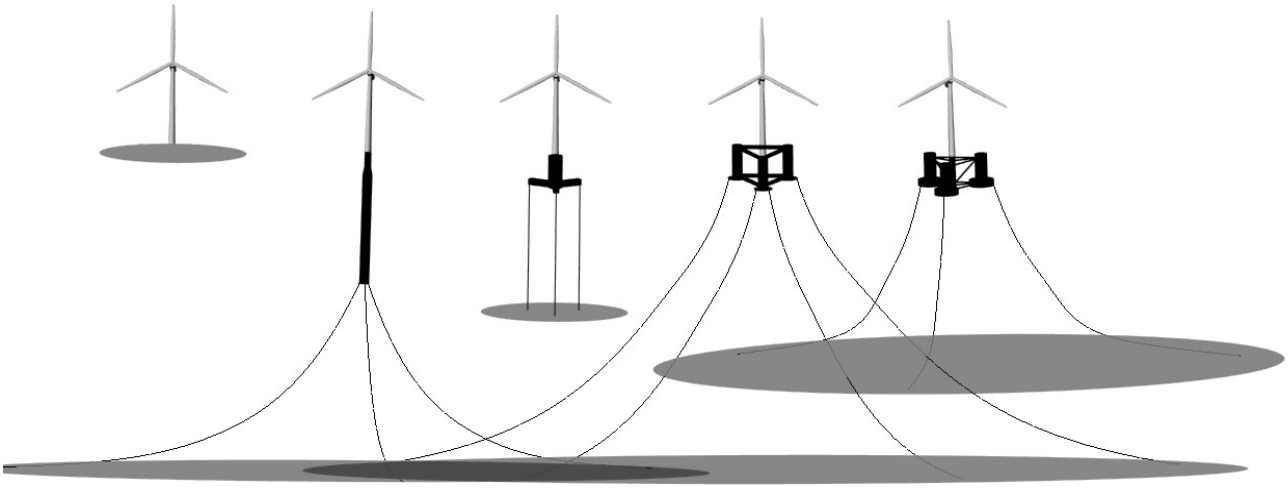

Figure 1: Wind turbine models (from left to right): land-based, spar, TLP, semi-submersible 1 (with offset turbine), and semi-submersible 2 (with turbine in middle).

2.1.1. Land-based

The NREL 5 MW wind turbine [15] with the OC3 Hywind tower [16] was selected as the benchmark land-based concept for this study. This wind turbine is a three-bladed, upwind, pitch-controlled turbine. The specifications are presented in Table 2. Using the OC3 Hywind tower (cantilevered at a height of 10m) allows for direct comparison with the floating models, but gives

Table 1: Floating wind turbines.

	Spar	TLP	Semi 1	Semi 2
Water depth (m)	320	150	320	200
Displacement (tonnes)	8227	5796	4619	14260
Hull mass (tonnes)	7466	2682	3810	13473
Draft (m)	120	22	17	20
Waterline diameter (m)	6.5	14.0	10.0[a]	12.0/6.5[b]
Surge natural period (s)	129.5	41.9	107.0	115.9
Sway natural period (s)	129.5	41.9	124.8	115.9
Heave natural period (s)	31.7	0.6	19.9	17.1
Roll natural period (s)	29.7	2.8	35.6	26.0
Pitch natural period (s)	29.7	2.8[c]	37.4	26.0
Yaw natural period (s)	8.2[d]	18.0	68.5	80.2
Tower bending period (s)	2.1	0.4[e]	2.3	2.4

[a] Single column

[b] Single offset column/Centre column

[c] Includes tower bending

[d] Low natural period in yaw is due to high yaw stiffness from the delta mooring configuration

[e] Second tower bending mode

the land-based turbine somewhat higher natural frequencies than the original NREL 5 MW baseline turbine [15].

Table 2: Land-based tower and turbine specifications [15, 16].

Parameter	Value
Type	Upwind/3 blades
Cut-in, rated and cut-out wind speed (m/s)	3, 11.4, 25
Hub height (m)	87.6
Rotor diameter (m)	126
Hub diameter (m)	3
Rotor mass (×1,000 kg)	110
Tower mass (×1,000 kg)	249.718
Nacelle mass (×1,000 kg)	240
Hub mass (×1,000 kg)	56.8

2.1.2. Spar

The OC3 Hywind spar platform, as defined by Jonkman [16], was included in the present study. Spar platforms are characterized by their large draft and small waterline area. Heavy ballast deep in the hull gives the platform its stability. In the global analysis, first order and viscous hydrodynamic forces as well as mean wave drift forces were applied and Newman's approximation was used to estimate the difference-frequency wave excitation. A catenary chain mooring system with delta lines and clump weights was applied to model the given mooring system stiffness [16]. The mooring lines were modelled using bar elements and connecting joints, allowing for a full dynamic solution.

2.1.3. TLP

TLPs are characterized by their vertical pre-tensioned tendons which provide stability. The pre-tension makes the platform stiff in heave, roll, and pitch, while still allowing for surge, sway, and yaw motions. In this study, the TLP hull was selected to be an approximately half-scale version of the original Sea Star oil platform [17]. Additional details regarding this TLP wind turbine design are provided by Bachynski and Moan [4], who identify it as TLPWT 3. Compared to other published TLP designs (e.g. [18, 19]), this design has relatively stiff tendons. As shown in Table 1, the TLP has lower hull mass and shorter natural periods than the other FWTs. For the global analysis, the tendons were modelled using axis-symmetric beam elements. Hydrodynamic forces on the tendons were applied using Morison's equation. For the hull, in addition to the first order and viscous forces, difference-frequency forces using Newman's approximation and sum-frequency forces due to the full second order potential solution were also applied. Due to limitations in the present version of the software, difference-frequency forces due to the full second order potential solution could not be applied simultaneously with the sum-frequency forces. There is no theoretical reason for not being able to apply both sum- and difference-frequency forces due to the full second order potential solution simultaneously; this is simply a limitation of the software at present. Since the sum-frequency forces are more critical for the platform response [20, 21] Newman's approximation was used for the difference frequency components.

2.1.4. Semi-submersible 1

Semi-submersibles are characterized by their large waterplane moment of inertia, which provides stability without requiring the deep draft of a spar platform. The platform natural periods are much longer than the first order wave periods. The first of two semi-submersible designs studied

here was similar, but not identical, to the generic WindFloat specification [22]. As in the WindFloat design, the wind turbine is placed on one of the offset columns. WindFloat has an active ballast system that counteracts the rotor's thrust force and reduces the mean platform pitch to nearly zero. The reaction time of this system is 20 minutes [22]. In the global analysis model, the ballast system was included by making the mass model a function of the mean wind speed, i.e. by giving different mass and restoring matrices for each environmental condition. The mass and restoring matrices were kept constant throughout each time domain simulation because the mean wind speed remained constant throughout the simulation. The ballast model in the simulations also counteracted the rotor torque moment. A multi-body hull model of semi-submersible 1 was used in the global analysis. The columns and heave plates were treated as rigid bodies, while the braces were modelled by flexible beams, following [23]. A detailed description of this model can be found in [24]. A long-term fatigue analysis of this concept is also presented in [25].

2.1.5. Semi-submersible 2

The second semi-submersible concept was the OC4 DeepCWind semi-submersible, as described in detail by Robertson et al. [26]. For this concept, the wind turbine is located on the centre column. There are three offset columns with pontoons around the centre column, each of which has an attached catenary mooring line. Braces are used to connect all of the columns as an integrated body. With approximately 3.5 times the hull mass of semi-submersible 1, semi-submersible 2 weighs in as the largest of the studied concepts in terms of both displacement and mass. For the global analysis, this concept was also modelled using a multi-body hull [23]. The four columns were modelled as rigid bodies, with first order and viscous hydrodynamic forces applied, while the braces were modelled as flexible beams with Morison-type loads. In this study, the orientation of the platform with respect to the wind is opposite that described by Robertson et al. [26, 27].

2.2. Drivetrain Model

In this paper, a 5 MW reference gearbox [12] has been used. This reference gearbox consists of three stages; two planetary and one parallel helical stage which was designed for the NREL 5 MW offshore reference wind turbine. It includes two main bearings to reduce the non-torque loads entering the gearbox. Table 3 presents the gearbox specifications. The layout, bearings and gears nomenclatures and topology are shown in Figures 2 and 3. The first torsional natural frequency of this reference drivetrain is about 2 Hz [15] which is modelled in the global analysis.

Post-Print Version. Original: https://doi.org/10.1016/j.marstruc.2015.03.006

Table 3: 5 MW reference gearbox specification [12].

Parameter	Value
Type	2 Planetary + 1 Parallel
1st stage ratio	1:3.947
2nd stage ratio	1:6.167
3rd stage ratio	1:3.958
Total ratio	1:96.354
Designed power (kW)	5000
Rated input shaft speed (rpm)	12.1
Rated generator shaft speed (rpm)	1165.9

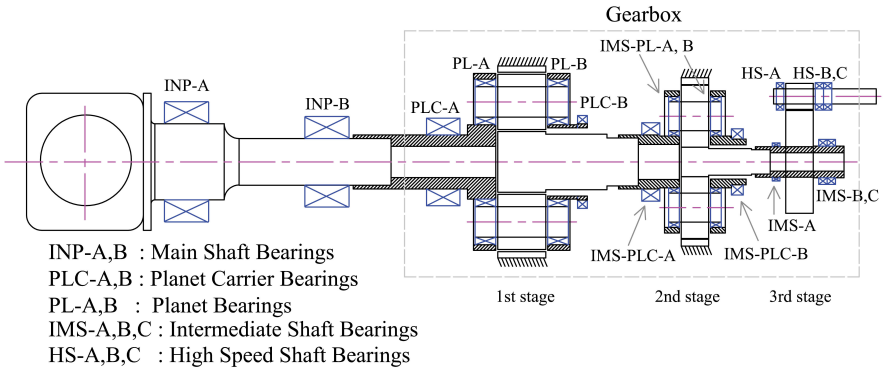

Figure 2: 5 MW reference gearbox schematic layout[12].

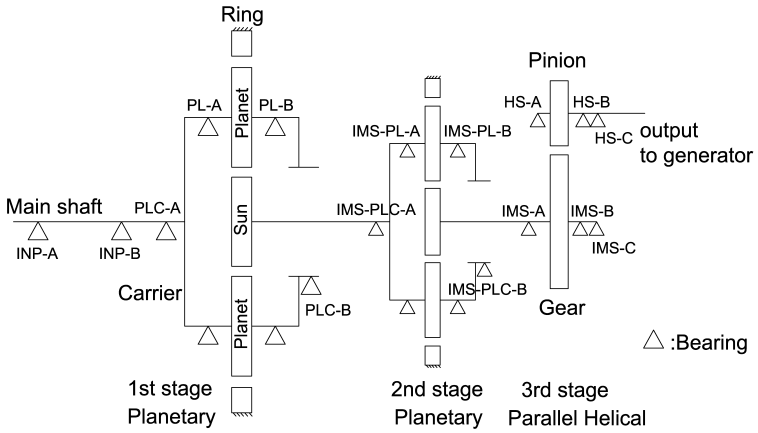

Figure 3: 5 MW reference gearbox topology[12].

3. Methodology

The dynamic loads applied on the drivetrain are obtained through a de-coupled analysis approach - see Fig. 4. The global analysis was first carried out in an aero-servo-hydrodynamic analysis tool and the forces and moments on the main shaft were obtained. These forces and moments together with drivetrain accelerations were then applied as input on a detailed drivetrain model and the local responses were measured. These steps are discussed in sections 3.1-3.3.

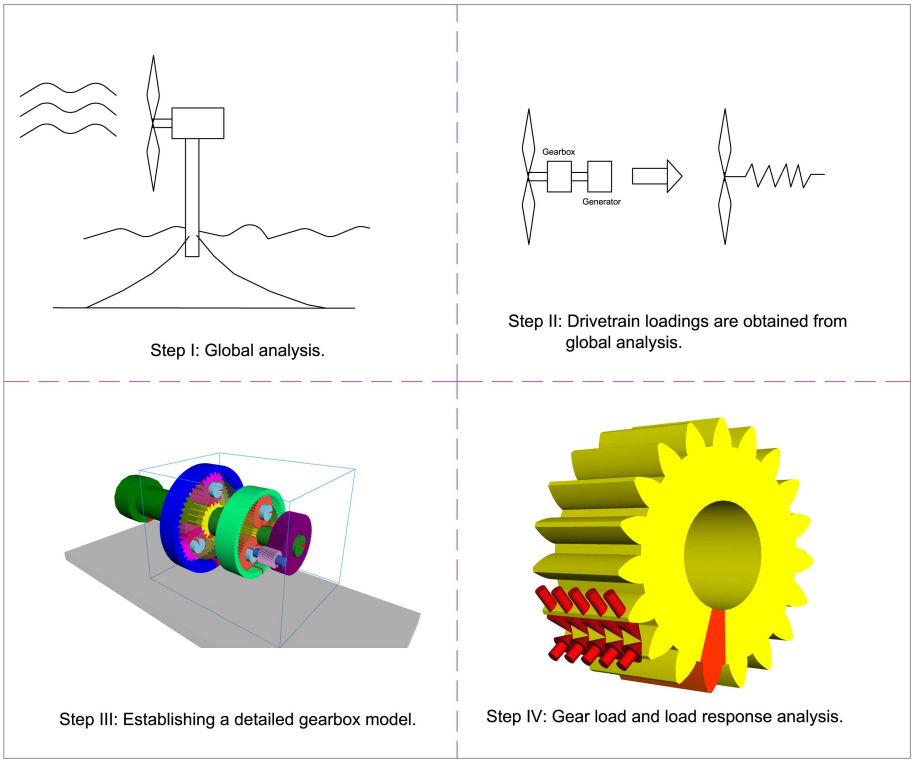

Figure 4: De-coupled approach for wind turbine gearbox analysis.

3.1. Global Analysis

Three integrated computer codes were used to model the global behaviour of the FWT systems in the time domain: SIMO, which models the rigid body hydrodynamics of the hull based on the input of frequency-domain hydrodynamic excitation and radiation loads from WAMIT as well as the viscous load from Morison's equation [28]; RIFLEX, which includes the finite element solver, flexible elements for the mooring lines (or tendons), tower, shaft, blades, and braces, and the link to an external controller [29]; and AeroDyn, which provides the forces and moments on the blades based on Blade Element/Momentum (BEM) or Generalized Dynamic Wake (GDW) theories, including dynamic stall, tower shadow, and skewed inflow correction [30]. The generator torque and blade pitch control system was written in Java. This combination provided a stable nonlinear finite element solver, sophisticated hydrodynamics, well-tested aerodynamics, and control logic. The SIMO-RIFLEX wind turbine module has been previously verified [31, 32], and the SIMO-RIFLEX-AeroDyn combination has been documented [33].

In the global analysis models, the hulls of the spar and TLP platforms were considered as rigid bodies, while the semi-submersibles were analyzed using multi-body hull models. The hydrody-

namic models of the concepts included a combination of potential flow and Morison's equation. The first order potential flow solution for each concept was computed using a panel model. The resulting added mass, radiation damping, and wave excitation were applied in the time domain using convolution. Additional viscous forces on large-volume components were included through the drag term in the Morison's equation. Morison's equation (including added mass, the Froude-Krylov and the diffraction forces) was also applied to slender elements such as braces and mooring lines which were not included in the panel model.

The aerodynamics model for the global analysis was chosen based on the wind speed. The BEM theory was applied for wind speeds lower than 8 m/s; otherwise the GDW theory was applied. At each time step in the dynamic simulation, aerodynamic loads were computed and applied to the structural model of the blades, which consisted of 17 nonlinear beam elements per blade.

The blade pitch control routines for FWTs are generally modified from those used on land-based turbines in order to avoid negative damping effect on platform resonant motions [34],[35]. In the present work, the OC3-Hywind control parameters were applied to the spar and semi-submersible wind turbines. Although the natural frequencies of the TLP are quite high, an intermediate control system was applied for the TLP wind turbine to avoid negative feedback in the wave frequency range. The control system parameters are given in Table 4. KI and KP are the integral and proportional coefficients for the blade pitch PI controller respectively. The controller natural frequency is $\omega_{\psi n}$.

Table 4: Control system parameters.

	Land-based	TLP	Spar, Semi-subs 1 and 2
KI	0.008069	0.003586	0.000896
KP (s)	0.018826	0.012551	0.006276
$\omega_{\psi n}$ (rad/s)	0.6	0.4	0.2
Above-rated strategy	constant power	constant torque	constant torque

A numerical hindcast model from the National and Kapodistrian University of Athens (NKUA) was used to generate 10-year statistics for several locations in the North Sea, Atlantic Ocean, and Mediterranean Sea for the Marina Platform project [36]. Six environmental conditions (ECs) based on the conditions near the Cabo Silleiro buoy off the coast of Portugal were selected for this study and for other comparisons [14]. Table 5 describes the characteristics of the waves (significant wave height H_s and peak period T_p) and wind (hub-height mean speed U and turbulence intensity I).

These conditions represent a range of operational conditions for the turbine, including low wind speeds which are likely to be encountered often.

Table 5: Environmental conditions.

	EC1	EC2	EC3	EC4	EC5	EC6
H_s (m)	2.0	4.5	5.0	5.0	4.0	5.5
T_p (s)	8.0	12.0	14.0	12.0	10.0	14.0
U (m/s)	4.0	7.0	10.0	12.0	14.0	20.0
I (-)	0.26	0.19	0.16	0.15	0.14	0.12
P(EC)(-)*	1.93×10^{-4}	1.99×10^{-4}	1.65×10^{-4}	1.86×10^{-4}	1.57×10^{-4}	1.12×10^{-4}

* P is given for a (0.73 m/s, 0.5 m, 0.5 s) box in the (U, H_s, T_p) space. The values given for (U, H_s, T_p) are the centres of boxes.

The JONSWAP wave model was used to generate the wave history with time step t=0.2s and frequency resolution $\Delta\omega = 2.4\times10^{-4}$ rad/s. The wind field was generated according to the Kaimal spectrum in TurbSim [37], using 32x32 points in the rotor plane with time step 0.05 seconds, and the normal turbulence model was applied for Class C turbines [38]. A power law vertical wind speed profile with exponent 0.14 was applied to the mean wind speed [39].

Finally, Table 5 also shows the probability of encountering the given conditions, where the probability P is given for a (0.73 m/s, 0.5 m, 0.5 s) box in the (U, H_s, T_p) space [25]. It should be noted that the chosen wave conditions represent relatively large waves for the given wind speeds, such that these conditions have relatively small probabilities. Conditions with relatively large waves were expected to show the most important differences between FWT concepts.

3.2. Drivetrain Load Effect Analysis

The reference gearbox was modelled in a multibody system (MBS) dynamic analysis tool, Simpack [40], as shown in Fig. 5. The MBS tool provides a powerful method for load effect analysis of wind turbine drivetrains and has been successfully used in earlier studies (e.g. [5, 41, 42, 43]). The gearbox in the MBS model consists of rigid or flexible bodies connected with appropriate force elements and joints. Gears are rigid with compliance at teeth while bearings are modelled with 6 DOF stiffness matrices. More details about the MBS modelling of wind turbine gearboxes are provided by Oyague [44] and Nejad et al. [12].

As shown in the Fig. 5, the forces and moments obtained from global analysis were applied on the main shaft. On the generator side, the generator speed was controlled to follow the same speed

calculated by the global analysis. The nacelle motions were also applied on the base plate for both floating wind turbines as well as the land-based. The MBS simulation was then carried out for 3800 sec. with sampling frequency of 200 Hz. The first 200 sec. of the results were discarded. Due to the long simulation time and high number of simulations, one simulation for each environmental condition was considered. In another study [6], the fatigue damage of gears and bearings in the 5 MW spar type wind turbine was carried out through six simulations. For a single environmental condition in that study, the difference in estimated fatigue based on a single simulation and six simulations was less than 10%. It is also important to note that the results presented in this paper are compared with the land-based case where the same wind (and wave) inputs are used for all conditions. In order to account for this uncertainty, only the comparison results above 10% are counted - see result section.

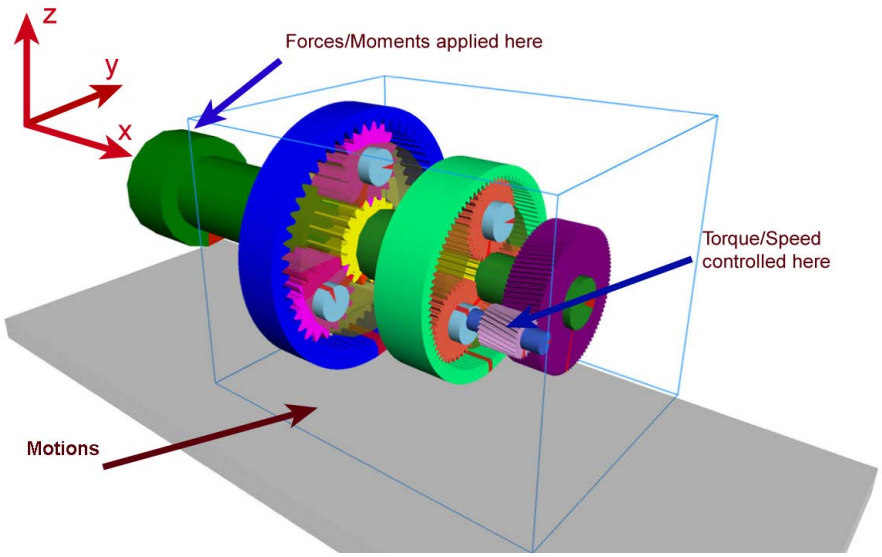

Figure 5: 5 MW gearbox MBS model [12].

3.3. Fatigue Damage Comparison

The dynamic forces obtained from the MBS model were then post-processed and the one hour fatigue damage in gears and bearings was calculated. For gears, the gear tooth root bending fatigue damage was calculated. Among the many failure modes of gears, tooth breakage can cause serious damage to the gearbox [41]. The gear tooth root bending stress was calculated based on the ISO 6336-3 method [45], then the one hour damage was obtained from [10]:

$$D = \frac{N}{K_c} \int_0^{+\infty} s^m f(s)\, ds = \frac{N}{K_c} A^m \Gamma \left(1 + \frac{m}{B}\right) \tag{1}$$

where $\Gamma()$ is the gamma function and A and B are the Weibull shape and scale parameters of the stress range distribution. N is the number of stress cycles in one hour and K_c and m are characteristic values from the gear SN curve. For the gears in this study, $m = 6.225$ and $\log_{10}(K_c) = 24.744$. The stress range number of cycles was calculated by the load duration distribution (LDD) method. For each bin, the stress range, s, starts from zero to the maximum stress in that bin. More details about this method and the gear tooth root fatigue damage calculation can be found in Nejad et al. [10].

Bearings are designed based on the desired life expressed by [8]:

$$L = (\frac{C}{P})^a \tag{2}$$

in which L is the bearing basic life defined as the number of cycles that 90% of an identical group of bearings achieve, under a certain test conditions, before the fatigue damage appears. C is the basic load rating and is constant for a given bearing. The parameter $a = 3$ for ball bearing and $a = \frac{10}{3}$ for roller bearings. P is the dynamic equivalent radial or thrust load calculated from [46]:

$$P = XF_r + YF_a \tag{3}$$

where F_a and F_r are the axial and radial loads on the bearing respectively and X and Y are constant factors obtained from the bearing manufacturer.

Equation 2 is one form of SN curve formulation; thus, one can estimate the bearing fatigue damage from [41]:

$$D = \sum_i \frac{l_i}{L_i} = \frac{1}{C^a} \sum_i l_i {P_i}^a \tag{4}$$

in this equation, l_i is the life (in number of cycles) used by the load range P_i and L_i is the life or number of cycles to the failure. More information on fatigue damage in wind turbine bearings can be found in [41, 11] and [42].

In the present work, the fatigue damage in gears and bearings of floating wind turbines is presented via comparison with the land-based turbine. This is expressed in percentage, χ, defined as:

$$\chi = \frac{D_{FL} - D_{LB}}{D_{LB}} \times 100 \tag{5}$$

where D_{LB} and D_{FL} are the fatigue damage in the land-based and floating turbines, respectively. Negative values of χ indicate that fatigue damage in the floating turbine is less than that of the land-based turbine for that particular component.

Post-Print Version. Original: https://doi.org/10.1016/j.marstruc.2015.03.006

4. Results & Discussion

It is important to ensure that all wind turbines follow the same - or similar - power curves before comparing the fatigue damages in the components. As it is presented in Figure 6, the mean power is almost equal for all the case study wind turbines. Note that the power loss is not considered in this figure.

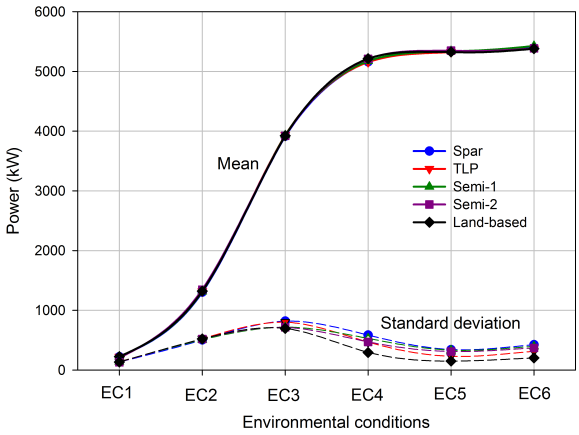

Figure 6: Power curve for spar, TLP, semi-1, semi-2 and land-based case study turbines.

It is also of interest to compare forces and moments in the main shaft of wind turbines. Figure 7 illustrates the mean and standard deviation of forces and moments in the main shaft of the spar, TLP, semi-1, semi-2 and land-based wind turbines for all environmental conditions. The coordinates used in this figure are shown in the Figure 5. F_X corresponds to the thrust force, while M_X corresponds to the torque. Figure 7 shows that the axial force in the main shaft appears to be the most affected parameter in floating wind turbines compared with the land-based wind turbine. The axial force in the spar wind turbine has the highest mean and standard deviation, as shown in Figure 7.

Comparisons of fatigue damage are made for all bearings. Many gearbox failures initiate at the bearings and are often those with high probability of fatigue failure. Comparisons are also made for two gears: the sun gear at first stage and the third pinion, these were selected based on the fatigue ranking procedure proposed by Nejad et al. [41]. Figure 8 illustrates the fatigue damage ranking of the components of the land-based 5 MW reference gearbox [12].

For the chosen components, the fatigue damage comparison factors χ—described in Equation 5—are presented in Tables 6, 7, 8 and 9 for the spar, semi-1, semi-2 and TLP respectively.

Post-Print Version. Original: https://doi.org/10.1016/j.marstruc.2015.03.006

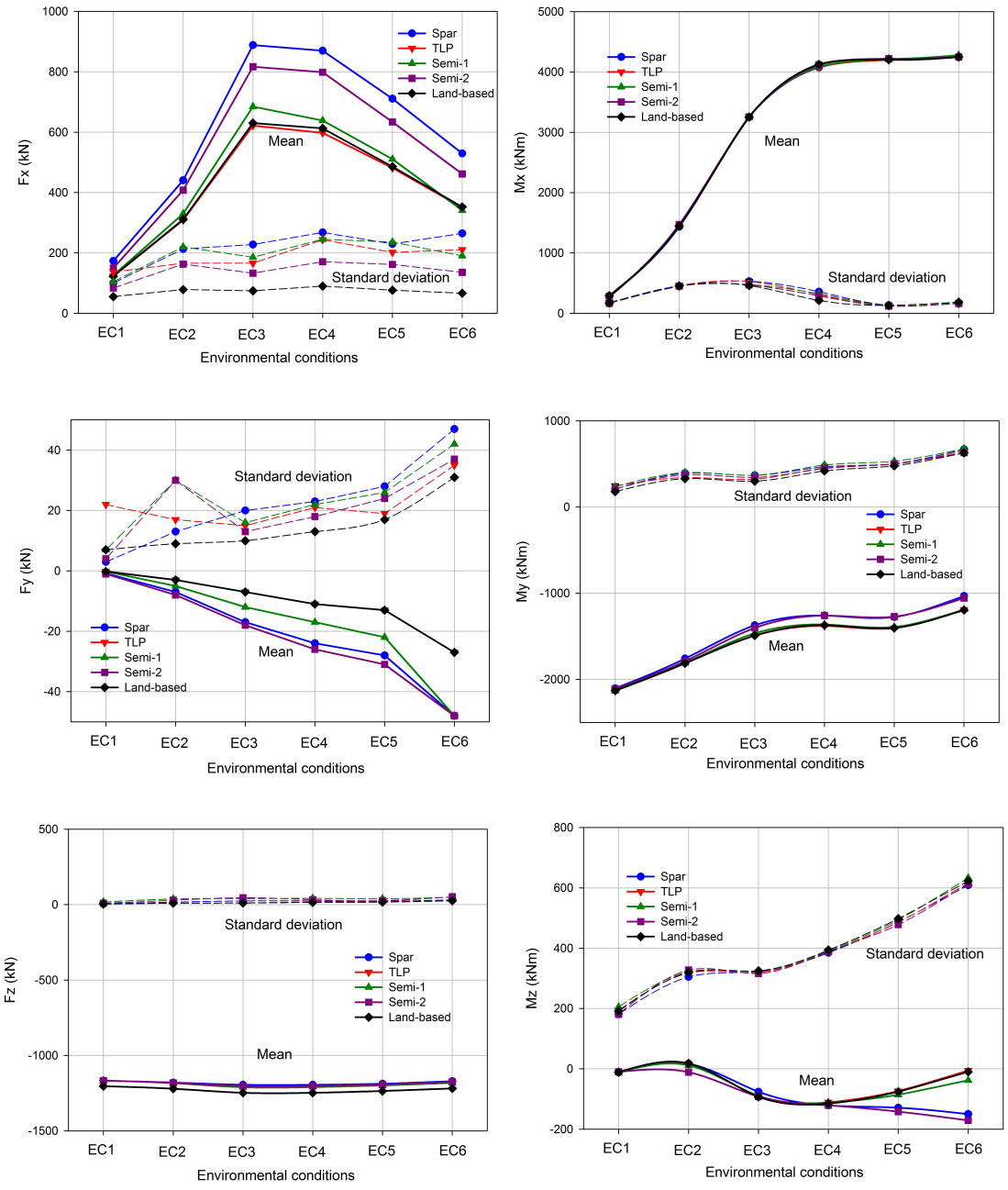

Figure 7: Mean and standard deviation of forces and moments applied on the main shaft in spar, TLP, semi-1, semi-2 and land-based turbines.

The bearings in the comparison tables are listed based on their locations in the gearbox, from the rotor to the generator side. As it was discussed earlier, the χ values between -10 to +10 are ignored. The red values indicate higher damage compared to the land-based turbine while the green values imply lower damages.

Post-Print Version. Original: https://doi.org/10.1016/j.marstruc.2015.03.006

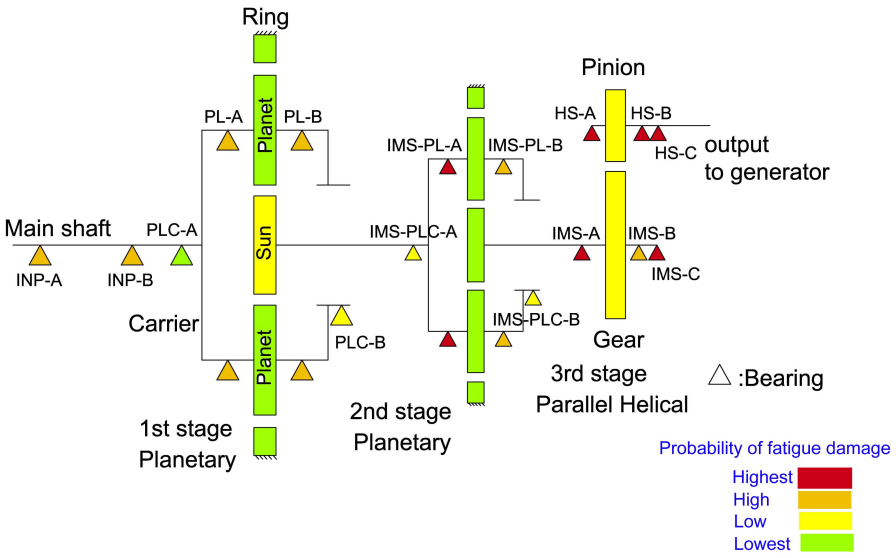

Figure 8: Gearbox "vulnerability map" or components fatigue damage ranking for the 5 MW land-based wind turbine [12].

Table 6: Spar: fatigue damage comparison factor, χ %.

Component	Description	EC1	EC2	EC3	EC4	EC5	EC6
INP-A	Main bearing, upwind	-8	-10	-17	-17	-19	-21
INP-B	Main bearing, downwind	35	175	179	205	210	280
PLC-A	1st stage planet carrier bearing, upwind	-4	-6	-15	-21	-18	-19
PLC-B	1st stage planet carrier bearing, downwind	-5	-8	-16	-16	-19	-20
PL-A	1st stage planet bearing, upwind	1	-1	4	-2	-1	0
PL-B	1st stage planet bearing, downwind	-4	-6	0	-4	-4	-4
IMS-PLC-A	2nd stage planet carrier bearing, upwind	-4	-6	-13	-16	-14	-14
IMS-PLC-B	2nd stage planet carrier bearing, downwind	-3	-4	-10	-14	-19	-29
IMS-PL-A	2nd stage planet bearing, upwind	-1	-2	5	-2	0	1
IMS-PL-B	2nd stage planet bearing, downwind	-2	-4	2	-3	-2	-1
IMS-A	Bearing on medium speed shaft	-2	-4	-3	-6	-6	-8
IMS-B	Bearing on medium speed shaft	-2	-3	1	-3	-3	-3
IMS-C	Bearing on medium speed shaft	-2	-2	2	-2	-2	-2
HS-A	Bearing on high speed shaft	-6	-3	4	-2	-1	0
HS-B	Bearing on high speed shaft	-5	-5	0	-3	-4	-3
HS-C	Bearing on high speed shaft	-5	-5	-1	-5	-4	-4
Sun gear	1st stage sun gear	-49	-9	11	-2	2	0
Pinion	3rd stage pinion	11	-11	11	-4	0	-2

The first impression of the results is that the second main bearing, INP-B, sustains more damage in all floating turbines than in the land-based turbine. INP-B supports both radial and axial forces. For this bearing the equivalent load, P, is calculated from equation 3 as $P = 0.67F_r + 3.6F_a$, thus any change in the axial force impacts significantly the equivalent load. As it is shown in Figure

Post-Print Version. Original: https://doi.org/10.1016/j.marstruc.2015.03.006

Table 7: Semi-1: fatigue damage comparison factor, χ %.

Component	Description	EC1	EC2	EC3	EC4	EC5	EC6
INP-A	Main bearing, upwind	-34	-5	-9	-6	-8	-5
INP-B	Main bearing, downwind	-23	74	42	45	56	40
PLC-A	1st stage planet carrier bearing, upwind	-31	0	-6	-1	-4	0
PLC-B	1st stage planet carrier bearing, downwind	-32	-2	-7	-3	-6	-2
PL-A	1st stage planet bearing, upwind	-27	1	2	0	1	6
PL-B	1st stage planet bearing, downwind	-29	-2	-2	-2	-2	1
IMS-PLC-A	2nd stage planet carrier bearing, upwind	-33	-1	-6	-3	-4	-1
IMS-PLC-B	2nd stage planet carrier bearing, downwind	-34	-3	-10	-11	-15	-22
IMS-PL-A	2nd stage planet bearing, upwind	-32	0	2	0	2	7
IMS-PL-B	2nd stage planet bearing, downwind	-33	-1	0	-1	0	4
IMS-A	Bearing on medium speed shaft	-31	-2	-4	-3	-3	-3
IMS-B	Bearing on medium speed shaft	-31	-1	-1	-1	-1	2
IMS-C	Bearing on medium speed shaft	-30	1	1	0	0	4
HS-A	Bearing on high speed shaft	-30	0	1	0	1	6
HS-B	Bearing on high speed shaft	-30	-3	-2	-2	-1	2
HS-C	Bearing on high speed shaft	-30	-3	-3	-3	-2	0
Sun gear	1st stage sun gear	-69	-6	4	-2	1	4
Pinion	3rd stage pinion	-83	-7	3	-3	0	2

Table 8: Semi-2: fatigue damage comparison factor, χ %.

Component	Description	EC1	EC2	EC3	EC4	EC5	EC6
INP-A	Main bearing, upwind	-7	-18	-16	-9	-12	-12
INP-B	Main bearing, downwind	16	79	88	119	114	115
PLC-A	1st stage planet carrier bearing, upwind	-3	-14	-15	-8	-12	-12
PLC-B	1st stage planet carrier bearing, downwind	-4	-16	-16	-9	-12	-12
PL-A	1st stage planet bearing, upwind	-12	-7	-4	5	5	6
PL-B	1st stage planet bearing, downwind	-15	-9	-2	9	7	4
IMS-PLC-A	2nd stage planet carrier bearing, upwind	-3	-14	-13	-3	-6	-5
IMS-PLC-B	2nd stage planet carrier bearing, downwind	-3	-16	-14	-5	-12	-24
IMS-PL-A	2nd stage planet bearing, upwind	-13	-7	-3	7	6	7
IMS-PL-B	2nd stage planet bearing, downwind	-12	-8	-2	9	8	6
IMS-A	Bearing on medium speed shaft	-5	-12	-7	4	2	0
IMS-B	Bearing on medium speed shaft	-7	-10	-4	7	5	4
IMS-C	Bearing on medium speed shaft	-11	-9	-3	8	6	6
HS-A	Bearing on high speed shaft	-21	-7	-2	9	7	7
HS-B	Bearing on high speed shaft	-18	-10	-5	6	4	3
HS-C	Bearing on high speed shaft	-19	-10	-5	5	4	2
Sun gear	1st stage sun gear	-57	8	3	1	2	-1
Pinion	3rd stage pinion	-53	3	1	0	0	-3

7 the axial load extends to a higher range in floating wind turbines than the land-based turbine, which explains the high damage observed for floating turbines. This also can be observed in the equivalent load and number of load cycles as presented in the Figure 9 - drawn for EC4. The

Table 9: TLP: fatigue damage comparison factor, χ %.

Component	Description	EC1	EC2	EC3	EC4	EC5	EC6
INP-A	Main bearing, upwind	-21	-6	-7	-3	-10	-9
INP-B	Main bearing, downwind	2	28	8	27	24	51
PLC-A	1st stage planet carrier bearing, upwind	-17	-2	-4	1	-7	-5
PLC-B	1st stage planet carrier bearing, downwind	-18	-4	-5	-1	-8	-6
PL-A	1st stage planet bearing, upwind	-2	3	5	1	-3	0
PL-B	1st stage planet bearing, downwind	-6	-3	0	-1	-6	-5
IMS-PLC-A	2nd stage planet carrier bearing, upwind	-16	-2	-4	1	-6	-5
IMS-PLC-B	2nd stage planet carrier bearing, downwind	-18	-4	-10	-10	-18	-26
IMS-PL-A	2nd stage planet bearing, upwind	-5	1	6	1	-2	1
IMS-PL-B	2nd stage planet bearing, downwind	-6	-1	3	0	-4	-2
IMS-A	Bearing on medium speed shaft	-16	-3	-2	-1	-7	-7
IMS-B	Bearing on medium speed shaft	-14	-1	2	0	-5	-4
IMS-C	Bearing on medium speed shaft	-10	0	3	2	-4	-2
HS-A	Bearing on high speed shaft	0	1	4	2	-3	0
HS-B	Bearing on high speed shaft	-7	-2	1	-1	-5	-4
HS-C	Bearing on high speed shaft	-6	-2	0	-2	-6	-5
Sun gear	1st stage sun gear	-57	0	12	-4	-1	-1
Pinion	3rd stage pinion	-72	-2	10	-5	-3	-3

INP-B sustains more damage in spar followed by semi-2, semi-1 and TLP wind turbines compared with the land-based turbine. For the spar wind turbine, the wave load is the primary cause of this large load variation in INP-B in below rated (EC2), rated (EC4) and above rated (EC5 and EC6) wind speeds, as illustrated in the power spectrum of the equivalent load in Figure 10. Note that the vertical axis is in logarithmic scale. "P" in this figure represents the rotor rotational frequency. According to this figure and for the semi-2 wind turbine, the rotational frequency "3P" has a higher contribution to the equivalent load than the wave in the below rated wind speed (EC2), while at the rated wind speed, wave influence is dominant. As the wind increases to the cut-out speed, the effect of "3P" increases.

In addition, the results show that the INP-B damage in semi-2 is higher than in semi-1 even though semi-2 is by far heavier than semi-1 platform. It appears that the active ballast system in semi-1 which counteracts the thrust force and reduces the platform pitch, contributes positively in thrust load reduction in semi-1.

The upwind main bearing (INP-A), which carries only radial load, has similar or less damage for all floating platforms compared with the land-based turbine. This implies that the radial force or its variation is lower in floating platforms than the land-based turbine. It is important to highlight that the fatigue damage in gears and bearings is not only a function of the load variation but also

Post-Print Version. Original: https://doi.org/10.1016/j.marstruc.2015.03.006

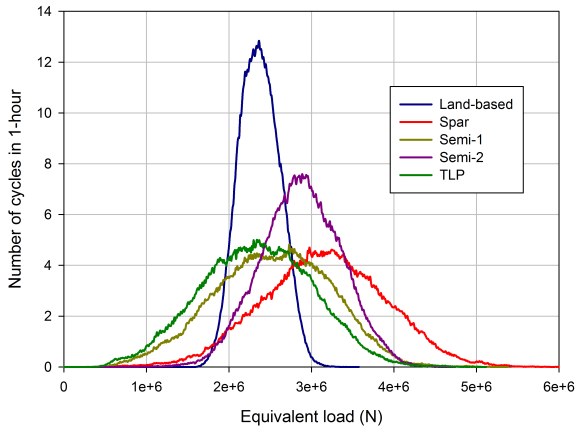

Figure 9: Downwind main bearing (INP-B). Equivalent load (equation 3) versus load cycles in floating and land-based turbines, shown for EC4.

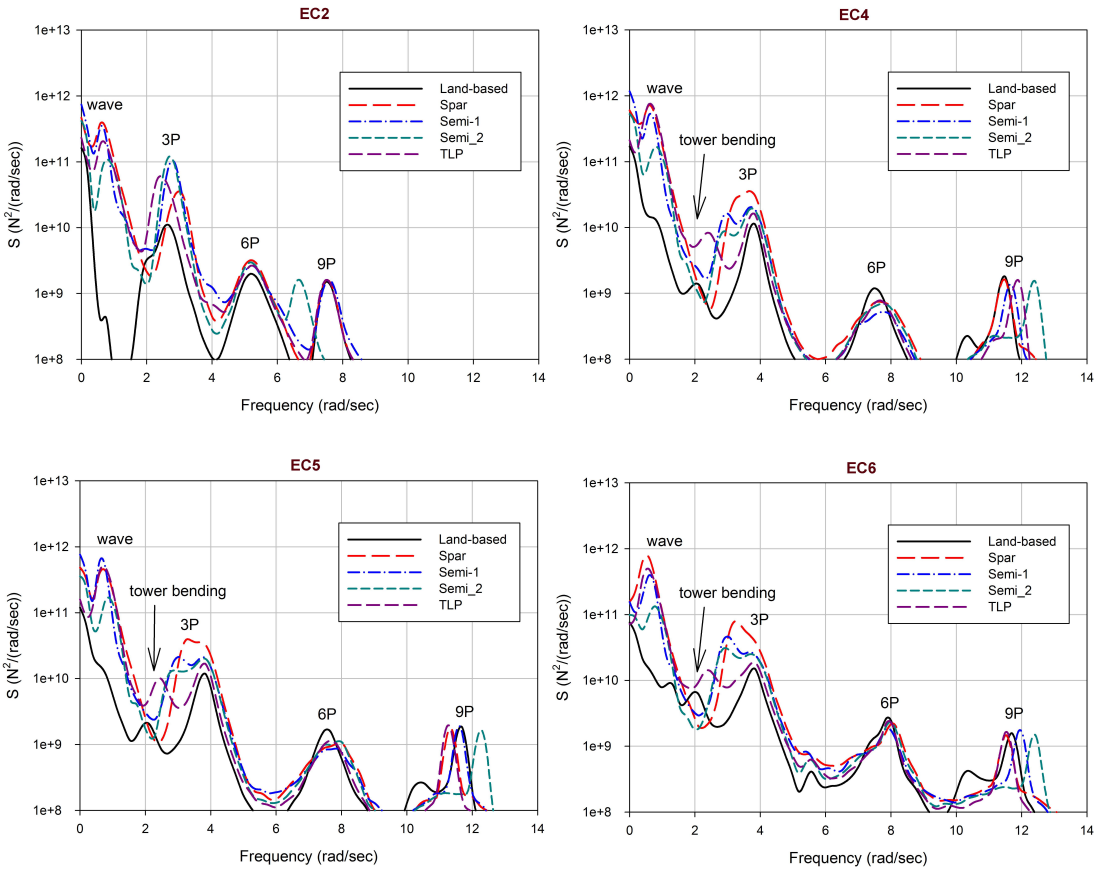

Figure 10: Downwind main bearing (INP-B). Spectrum of equivalent load (equation 3) for EC2, EC4, EC5 and EC6.

is a function of the load mean value. In every rotation a single gear tooth or a roller in the bearing undergoes a stress cycle from zero to a peak value irrespective whether the input load is constant or it varies. The stress cycle of the gear tooth or bearing roller does not explicitly correspond to the load fluctuations. This is due to the fact that the gear or bearing stress range is not only a function of the external load fluctuations but also it is a function of the rotational speed [10].

Apart from the main bearings, INP-A and INP-B, which are located outside the gearbox on the main shaft, all other bearings are situated inside the gearbox. The comparison shows that these bearings hold equal or even lower damage in floating wind turbines. In the spar wind turbine and from rated and above rated wind speed some of these bearings inside the gearbox enjoy lower damage than in the land-based wind turbine. There are more bearings with low damage for the semi-2 wind turbine in both low and high wind speeds, while the semi-1 wind turbine - the one with the wind turbine on an offset column - appears to be more "drivetrain friendly" at low wind speed. However, it is important to note that the semi-1 is far lighter than the semi-2 turbine with a displacement of almost 30% of the semi-2 and is equipped with an active ballast system. Finally, bearings in the TLP appear to hold very similar damages to the land-based turbine.

Moreover, many green values in EC1 imply that the semi-1 and TLP turbines perform better at this low environmental condition than the land-based turbine. EC1 is the environmental condition near the cut-in wind speed.

For the two selected gears, it appears that they sustain almost equal damage in floating and land-based turbines. This is mainly due to the two main bearings design which has reduced the non-torque loads imposed on the gears. Moreover, bearings are more critical than gears in this gearbox as shown in the Figure 8.

5. Conclusions

In this paper a land-based designed 5 MW drivetrain was modelled on four types of floating support structures: spar, TLP and two semi-submersibles, and the fatigue damage in mechanical components was compared for different environmental conditions. All wind turbines followed an identical power curve, to ensure the consistency in comparisons. The comparison of fatigue damage in the drivetrain of floating versus land-based wind turbines reveals that the main bearing carrying axial loads sustains more damage in floating wind turbines than land-based. The spar floating wind turbine is the one with the highest damage on the main bearing followed by semi-2, semi-1 and

TLP wind turbine. The main reason for the higher damage in the spar wind turbine is the large wave induced axial force on the main shaft. The main bearing damage in the spar wind turbine is observed to be significant, almost three times more than the land-based in high wind speeds.

Overall, the comparison results suggest that other gears and bearings inside the gearbox - apart from main bearings which are situated outside the gearbox - perform equal to or even better in floating wind turbines than land-based. Moreover, the limited simulations presented in this study suggest that the gearbox damage is almost equal in the TLP and the land-based and for some bearings in the spar, semi-1 and semi-2 it is even lower than the land-based.

It is emphasized that the reference gearbox used in this study includes two main bearings, which largely reduce non-torque loads entering the gearbox, thus, the conclusions should not be generalized as they are very much dependent to the drivetrain configuration. Furthermore, a limited number of environmental conditions have been studied. Therefore, it is recommended to further devote analyses of different types of drivetrains on the selected floating support structures in various environmental conditions.

Acknowledgement

The authors wish to acknowledge the financial support from Research Council of Norway through Norwegian Research Centre for Offshore Wind Technology (Nowitech) and Centre for Ships and Ocean Structures (CeSOS).

References

[1] Jonkman J. Dynamics of offshore floating wind turbines-model development and verification. *Wind Energy*, 12(5):459–492, 2009.

[2] Karimirad M., Meissonnier Q., Gao Z., and Moan T. Hydroelastic code-to-code comparison for a tension leg spar-type floating wind turbine. *Marine Structures*, 24(4):412–435, 2011.

[3] Karimirad M. and Moan T. A simplified method for coupled analysis of floating offshore wind turbines. *Marine Structures*, 27(1):45–63, 2012.

[4] Bachynski EE. and Moan T. Design considerations for tension leg platform wind turbines. *Marine Structures*, 29(1):89–114, 2012.

[5] Xing Y., Karimirad M., and Moan T. Modelling and analysis of floating spar-type wind turbine drivetrain. *Wind Energy*, 17(4):565–587, 2014.

[6] Nejad AR., Bachynski EE., Gao Z., and Moan T. Fatigue damage comparison of mechanical components in a land-based and a spar floating wind turbine. *Procedia Engineering*, 101:330–338, 2015.

[7] Kaldellis J.K. and Zafirakis D.P. Trends, prospects and R&D directions in wind turbine technology. In Ali Sayigh, editor, *Comprehensive Renewable Energ*, pages 671–724. Elsevier, 2012.

[8] IEC 61400-4. Wind turbines, part 4: Standard for design and specification of gearboxes, 2012.

[9] Dong W., Xing Y., Moan T., and Gao Z. Time domain-based gear contact fatigue analysis of a wind turbine drivetrain under dynamic conditions. *International Journal of Fatigue*, 48:133–146, 2013.

[10] Nejad AR., Gao Z., and Moan T. On long-term fatigue damage and reliability analysis of gears under wind loads in offshore wind turbine drivetrains. *International Journal of Fatigue*, 61:116–128, 2014.

[11] Jiang Z., Xing Y., Guo Y., Moan T., and Gao Z. Long-term contact fatigue analysis of a planetary bearing in a land-based wind turbine drivetrain. *Wind Energy*, doi:10.1002/we.1713, 2014.

[12] Nejad AR., Guo Y., Gao Z., and Moan T. Definition of a 5-MW reference gearbox for offshore wind turbine development. *submitted for publication*, 2014.

[13] Bachynski EE., Etemaddar M., Kvittem M., Luan C., and Moan T. Dynamic analysis of floating wind turbines during pitch actuator fault, grid loss, and shutdown. *Energy Procedia*, 35:210–222, 2013.

[14] Bachynski EE., Kvittem M., Luan C., and Moan T. Wind-wave misalignment effects on floating wind turbines: motions and tower load effects. *Journal of Offshore Mechanics and Arctic Engineering*, 136(4):0419021–04190212, 2014.

[15] Jonkman J., Butterfield S., Musial W., and Scott G. Definition of a 5-MW reference wind turbine for offshore system development. Technical Report NREL/TP-500-38060, National Renewable Energy Laboratory (NREL), 2009.

[16] Jonkman J. *Definition of the Floating System for Phase IV of OC3*. National Renewable Energy Laboratory, 2010.

[17] Kibbee S., Leverette S., Davies K., and Matten R. Morpeth SeaStar Mini-TLP. In *Proceeding of Offshore Technology Conference, Paper No. OTC 10855*. Offshore Technology Conference, Houston, Texas, 3-6 May 1999.

[18] Matha D. Model development and loads analysis of an offshore wind turbine on a tension leg platform with a comparison to other floating turbine concepts: April 2009. Technical report, National Renewable Energy Laboratory (NREL), Golden, CO., 2010.

[19] Stewart G., Lackner M., Robertson A., Jonkman J., and Goupee A. Calibration and validation of a FAST floating wind turbine model of the deepcwind scaled tension-leg platform. In *Proc. 22nd International Offshore and Polar Engineering Conference*, pages 380–387, 2012.

[20] Roald L., Jonkman J., Robertson A., and Chokani N. The effect of second-order hydrodynamics on floating offshore wind turbines. *Energy Procedia*, 35:253–264, 2013.

[21] Bachynski EE. and Moan T. Hydrodynamic modeling of tension leg platform wind turbines. In *ASME 2013 32nd International Conference on Ocean, Offshore and Arctic Engineering*, pages V008T09A003–V008T09A003. American Society of Mechanical Engineers, 2013.

[22] Roddier D., Peiffer A., Aubault A., and Weinstein J. A generic 5 MW windfloat for numerical tool validation and comparison against a generic spar. In *ASME 2011 30th International Conference on Ocean, Offshore and Arctic Engineering*, pages 247–255. American Society of Mechanical Engineers, 2011.

[23] Luan C., Gao Z., and Moan T. Modelling and analysis of a semi-submersible wind turbine with a central tower with emphasis on the brace system. In *ASME 2013 32nd International Conference on Ocean, Offshore and Arctic Engineering*, pages V008T09A024–V008T09A024. American Society of Mechanical Engineers, 2013.

[24] Kvittem M. *Modelling and Response Analysis for Fatigue Design of a Semi-Submersible Wind Turbine*. Ph.D thesis, Department of Marine Technology, Norwegian University of Science and Technology, 2014.

[25] Kvittem M. and Moan T. Time domain analysis procedures for fatigue assessment of a semi-submersible wind turbine. *Marine Structures*, 40:38–59, 2015.

[26] Robertson A., Jonkman J., Masciola M., Song H., Goupee A., Coulling A., and Luan C. Definition of the semisubmersible floating system for Phase II of OC4. *IEA OC4 Report*, 2012.

[27] Robertson A., Jonkman J., Musial W., Vorpahl F., and Popko W. Offshore code comparison collaboration, continuation: Phase II results of a floating semisubmersible wind system. report no.: NREL/CP-5000-60600. Technical report, National Renewable Energy Laboratory (NREL), 2013.

[28] MARINTEK. *SIMO User's Manual*. MARINTEK, 2011.

[29] MARINTEK. *RIFLEX User's Manual*. MARINTEK, 2011.

[30] Moriarty PJ. and Hansen AC. *AeroDyn Theory Manual*. National Renewable Energy Laboratory (NREL), 2005.

[31] Luxcey N., Ormberg H., and Passano E. Global analysis of a floating wind turbine using an aero-hydro-elastic numerical model: Part 2–benchmark study. In *ASME 2011 30th International Conference on Ocean, Offshore and Arctic Engineering*, pages 819–827. American Society of Mechanical Engineers, 2011.

[32] Ormberg H., Passano E., and Luxcey N. Global analysis of a floating wind turbine using an aero-hydro-elastic model: Part 1–code development and case study. In *ASME 2011 30th International Conference on Ocean, Offshore and Arctic Engineering*, pages 837–847. American Society of Mechanical Engineers, 2011.

[33] Ormberg H. and Bachynski EE. Global analysis of floating wind turbines: Code development, model sensitivity and benchmark study. In *22nd International Ocean and Polar Engineering Conference*, volume 1, pages 366–373, 2012.

[34] Skaare B., Hanson TD., Nielsen FG., Yttervik R., Hansen AM., Thomsen K., and Larsen TJ. Integrated dynamic analysis of floating offshore wind turbines. In *2007 European Wind Energy Conference and Exhibition*, 2007.

[35] Larsen TJ. and Hanson TD. A method to avoid negative damped low frequent tower vibrations for a floating, pitch controlled wind turbine. *Journal of Physics: Conference Series*, 75(1):012073, 2007.

[36] Li L., Gao Z., and Moan T. Joint environmental data at five european offshore sites for design of combined wind and wave energy devices. In *ASME 2013 32nd International Conference on Ocean, Offshore and Arctic Engineering*, pages V008T09A006–V008T09A006. American Society of Mechanical Engineers, 2013.

[37] Jonkman J. *TurbSim User's Guide*. National Renewable Energy Laboratory (NREL), 2009.

[38] IEC 61400-1. Wind turbines, part 1: Design requirements, 2005.

[39] IEC 61400-3. Wind turbines, part 3: Design requirements for offshore wind turbines, 2009.

[40] SIMPACK. Multi body system software. `www.simpack.de/`. [Online; accessed 03-April-2014].

[41] Nejad AR., Gao Z., and Moan T. Fatigue reliability-based inspection and maintenance planning of gearbox components in wind turbine drivetrains. *Energy Procedia*, 53:248–257, 2014.

[42] Nejad AR., Xing Y., Guo Y., Keller J., Gao Z., and Moan T. Effect of floating sun gear in wind turbine planetary gearbox with geometrical imperfections. *Wind Energy*, doi:10.1002/we.1808, 2014.

[43] Nejad AR., Odgaard PF., Gao Z., and Moan T. A prognostic method for fault detection in wind turbine drivetrains. *Engineering Failure Analysis*, 42:324–336, 2014.

[44] Oyague F. Gearbox modelling and load simulation of a baseline 750-kW wind turbine using state-of-the-art simulation codes. Technical Report NREL/TP-500-41160, National Renewable Energy Laboratory (NREL), 2009.

[45] ISO 6336-3. Calculation of load capacity of spur and helical gears, part 3: Calculation of tooth bending strength, 2006.

[46] Lundberg G. and Palmgren A. Dynamic capacity of roller bearings. *Acta Polytechnica Mechanical Engineering Series*, 2:5–32, 1952.